Acid secretion by mitochondrion-rich cells of medaka (Oryzias latipes) acclimated to acidic freshwater

Chia-Cheng Lin, Li-Yih Lin, Hao-Hsuan Hsu, Violette Thermes, Patrick Prunet, Jiun-Lin Horng, Pung-Pung Hwang

Am J Physiol Regul Integr Comp Physiol 302: R283–R291, 2012.
First published November 2, 2011; doi:10.1152/ajpregu.00483.2011.

Acid secretion by mitochondrion-rich cells of medaka (*Oryzias latipes*) acclimated to acidic freshwater

Chia-Cheng Lin,[1] Li-Yih Lin,[2] Hao-Hsuan Hsu,[1] Violette Thermes,[3] Patrick Prunet,[4] Jiun-Lin Horng,[5,*] and Pung-Pung Hwang[1,*]

[1]*Institute of Cellular and Organismic Biology, Academia Sinica, Taipei, Taiwan, Republic of China;* [2]*Department of Life Science, National Taiwan Normal University, Taipei, Taiwan, Republic of China; and* [3]*Institut National de la Recherche Agronomique, Station Commune de Recherches en Ichtyophysiologie, Biodiversité et Environnement, Campus de Beaulieu, Rennes, France;* [4]*Institut National de la Recherche Agronomique, UR1037, SCRIBE, IFR140, Biogenouest, Rennes, France; and* [5]*Department of Anatomy, Taipei Medical University, Taipei, Taiwan, Republic of China*

Submitted 29 August 2011; accepted in final form 30 October 2011

Lin CC, Lin LY, Hsu HH, Thermes V, Prunet P, Horng JL, Hwang PP. Acid secretion by mitochondrion-rich cells of medaka (*Oryzias latipes*) acclimated to acidic freshwater. *Am J Physiol Regul Integr Comp Physiol* 302: R283–R291, 2012. First published November 2, 2011; doi:10.1152/ajpregu.00483.2011.—In the present study, medaka embryos were exposed to acidified freshwater (pH 5) to investigate the mechanism of acid secretion by mitochondrion-rich (MR) cells in embryonic skin. With double or triple in situ hybridization/immunocytochemistry, the Na^+/H^+ exchanger 3 (NHE3) and H^+-ATPase were localized in two distinct subtypes of MR cells. NHE3 was expressed in apical membranes of a major proportion of MR cells, whereas H^+-ATPase was expressed in basolateral membranes of a much smaller proportion of MR cells. Gill mRNA levels of NHE3 and H^+-ATPase and the two subtypes of MR cells in yolk sac skin were increased by acid acclimation; however, the mRNA level of NHE3 was remarkably higher than that of H^+-ATPase. A scanning ion-selective electrode technique was used to measure H^+, Na^+, and NH_4^+ transport by individual MR cells in larval skin. Results showed that Na^+ uptake and NH_4^+ excretion by MR cells increased after acid acclimation. These findings suggested that the NHE3/Rh glycoprotein-mediated Na^+ uptake/NH_4^+ excretion mechanism plays a critical role in acidic equivalent (H^+/NH_4^+) excretion by MR cells of the freshwater medaka.

ionocytes; Na^+/H^+ exchanger; Rh glycoprotein

IN MAMMALS, METABOLIC ACIDS are mainly excreted by proximal tubules of the kidneys, and about 60% of H^+ secretion is mediated by the Na^+/H^+ exchanger (NHE). NHE3 mediates ~50% of the overall apical NHE activity of proximal tubules for H^+ secretion, which is also the first step in bicarbonate reabsorption (5, 45). Mice with targeted disruption of NHE3 exhibited metabolic acidosis and decreased renal absorption of Na^+, fluids, and HCO_3^-. Furthermore, animals given a chronic acid load showed increased NHE3 activity and protein in both proximal tubules and thick ascending limbs of the loop of Henle (5). On the other hand, in the epididymis, acidification of luminal fluid is essential for sperm maturation, sperm storage, and fertility. Previous studies mainly focused on the role of H^+-ATPase in acid secretion; however, experiments on an NHE3 inhibitor and NHE3-deficient mice recently showed the important role of NHE3 in luminal acidification (32). All of these studies indicate the essential function of NHE3 in acid excretion in mammals.

In freshwater fish, gills account for more than 90% of the acid-base regulation function. In fish embryos, the acid-excreting function is performed by the embryonic skin. Using zebrafish embryonic skin for acid-base regulation studies, researchers have proven that metabolic acid excretion is mainly conducted by H^+-ATPase-rich (HR) cells, a subtype of mitochondrion-rich (MR) cells, with an increased cell number and H^+-secreting function after acid acclimation (18, 19, 29). In rainbow trout (*Oncorhynchus mykiss*), H^+-ATPase-expressing peanut agglutinin $(PNA)^-$ MR cells responded to a hypercapnic stimulus and were believed to function in acid excretion (15).

NHE3 was also found to be expressed in zebrafish HR cells and medaka MR cells, and treatment with an NHE inhibitor decreased Na^+ uptake by those cells (48, 49). Upregulation of both the Na^+ uptake function and NHE expression was also reported in tilapia under low-Na^+ freshwater (FW) experimental conditions (24). Recent studies on medaka demonstrated that the NH_4^+-dependent Na^+ uptake by MR cells relies on the coupling of the Rh glycoprotein (Rhcg1) and NHE3 (48). In addition, other studies have proposed the important role of NHE3 in acid excretion by MR cells in FW teleosts. In Osorezan dace (*Tribolodon hakonensis*) and tilapia (*Oreochromis mossambicus*), NHE3 was expressed in the apical membrane of gill MR cells, and its expression and/or cell number increased during acclimation to acidic FW (14, 16). In rainbow trout, both NHE2 and NHE3 are expressed in PNA^+ MR cells, and only NHE2 mRNA increased after hypercapnic acidosis (25); however, PNA^+ MR cells were previously proposed to be base-secreting MR cells (15, 25, 34). Taken together, our current understanding of the functional role of NHEs in acid-secreting mechanisms of teleosts in FW is still fragmentary and needs further exploration.

In this study, we used FW-acclimated euryhaline medaka as a model to test our hypothesis that NHE plays a major role in acid-secretion function during acclimation to acidic FW. Experiments were designed to answer several specific questions: *1*) Are NHE3 or NHE2 (or both) and H^+-ATPase expressed in specific groups of MR cells?; *2*) are the expressions of NHE2/3, H^+-ATPase, and Rhcg1 regulated during acclimation to acidic FW? Does an acidic environment affect cell densities of acid-secreting MR cells?; and *3*) are ionic (H^+, NH_4^+, and Na^+) transports by MR cells regulated during acclimation to acidic FW?

* J.-L. Horng and P.-P. Hwang contributed equally to this study.

Address for reprint requests and other correspondence: P.-P. Hwang, Institute of Cellular and Organismic Biology, Academia Sinica, Taipei, Taiwan, ROC. (e-mail: pphwang@gate.sinica.edu.tw).

MATERIALS AND METHODS

Experimental animals. Mature Japanese medaka (*Oryzias latipes*) were reared in tanks with circulating tap water at 27°C with a 14:10-h light-dark photoperiod. Females spawned every day, and fertilized egg clusters were collected from the belly of females and rinsed with running tap water to remove any sludge and separate the clusters into single eggs. The eggs were incubated in different artificial FWs for specific experiments. Embryos usually hatched at 7–8 days postfertilization (dpf), and newly hatched larvae were used for the following experiments. During the experiments, the embryos were not fed, and the freshwater was changed daily to ensure optimal water quality. The experimental protocols were approved by the Academia Sinica Institutional Animal Care and Utilization Committee (approval no.: RFiZOOHP2009060).

Acclimation experiments. All of the incubating solutions were prepared by adding various salts (Sigma-Aldrich, St. Louis, MO) to double-distilled water. The FW contained (in mM) 0.5 NaCl, 0.2 $CaSO_4$, 0.2 $MgSO_4$, 0.16 KH_2PO_4, and 0.16 K_2HPO_4 (pH 7.0). Acidified FW was produced by adjusting FW to pH 5 with H_2SO_4 for embryo acidic acclimation. For the acidic acclimation of adult medaka, acidic FW was adjusted to pH 4. Embryonic and adult medaka were acclimated for 7 and 14 days, respectively, to acidic FW and FW, and all showed normal behaviors with no mortality during the acclimation period. During the experiments, acidic FW was continuously pumped into the experimental tank bottom with an electrical pump to maintain a stable pH. pH values of the experimental media were checked with a pH meter (Mettler Toledo MP225, Schwerzenbach, Switzerland).

Preparation of total RNA. Gills from 6 individuals were collected and homogenized in TRIzol reagent (Ambion, Woodward, TX). Total RNA was purified following the manufacturer's protocol. The total amount of RNA was determined at absorbances of 260 and 280 nm by spectrophotometry (ND-1000, NanoDrop Technology, Wilmington, DE). All RNA pellets were stored at −20°C.

RT-PCR. For cDNA synthesis, 5 μg of total RNA was reverse-transcribed in a final volume of 20 μl containing 0.5 mM dNTPs, 2.5 μM oligo$(dT)_{20}$, 5 mM dithiothreitol, 40 units of an RNase inhibitor, and 200 units of SuperScript III RT (Invitrogen, Carlsbad, CA) for 1.5 h at 55°C, followed by incubation at 70°C for 15 min. Then 20 units of *Escherichia coli* RNase H (Invitrogen, Carlsbad, CA) were added to remove the remnant RNA with a 20-min incubation at 37°C. For PCR amplification, 1 μl of cDNA was used as a template in a 25-μl final reaction volume containing 0.25 μM dNTP, 1.25 units of Gen-Tag polymerase (Genemark, Taipei, Taiwan), and 0.2 μM of each primer. The primer sets are shown in Table 1.

Molecular cloning and sequencing analysis. Partial open reading frames of medaka *slc9a, slc9a3,* and *atp6v1a* homologs obtained from the genome were carefully confirmed with the expressed sequence tag database. Specific primers were designed for cloning and the RT-PCR analysis. Thus, PCR products obtained were subcloned into a pGEM-T Easy vector (Promega, Madison, WI), and the nucleotide sequences were determined with an ABI 377 sequencer (Applied Biosystems, Warrington, UK). Sequence analysis was conducted with the BLASTx program (NCBI).

Quantitative qRT-PCR. mRNA expression levels of forkhead box I 3 (*foxi3*; Ref. 39), NHE2 (*slc9a2*, ENSORLG00000012399; recently reannotated as NHE4 by Ensembl), NHE3 (*slc9a3*, ENSORLG 00000009128), V-type H^+-ATPase V1 subunit A (*atp6v1a*, ENSO RLG00000006642), and Rhcg1 (48) were measured by a qRT-PCR with a Roche Lightcycler 480 (Roche, Penzberg, Germany). The sample in each well had a final volume of 10 μl and contained 5 μl of 2 × SYBR Green master mix (Roche), 3.2 ng of cDNA, and 50 nM of primers pairs. The standard curve of each gene was checked in a linear range with ribosomal protein (RP)L7 as an internal control. Primer sets for the qRT-PCR are given in Table 1. The specificity of the primer sets that we used was confirmed by the presence of a single band of correct size on gel electrophoresis. In addition, the presence of a single peak in the dissociation curve analysis represented the specific product expected from the primer pair.

Whole-mount in situ hybridization. The *slc9a2*, *slc9a3,* and *atp6v1a* fragments were obtained by a PCR and inserted into the pGEM-T Easy vector (Promega, Madison, WI). The inserted fragments were amplified with the T7 and SP6 primers by PCR, and the products were used as templates for in vitro transcription with T7 and SP6 RNA polymerase (Roche) in the presence of digoxigenin (DIG)-UTP (Roche) to synthesize sense and anti-sense probes, respectively. DIG-labeled RNA probes were examined using RNA gels, and a dot blot assay was used to confirm their quality and concentrations. Medaka embryos were anesthetized on ice and fixed with 4% paraformaldehyde in a PBS (1.4 mM NaCl, 0.2 mM KCl, 0.1 mM Na_2HPO_4, and 0.002 mM KH_2PO_4; pH 7.4) solution at 4°C overnight. Afterward, samples were washed with diethylpyrocarbonate-PBST (PBS with 0.1% Tween-20) several times (for 10 min each). After PBST washing, samples were incubated with hybridization buffer (HyB, 50% formamide, 5× SSC, and 0.1% Tween 20) at 65°C for 5 min and with HyB containing 500 μg/ml yeast tRNA at 65°C for 4 h before hybridization. After overnight hybridization with 100 ng/ml DIG-labeled antisense or sense RNA probes, embryos were serially washed with 2 × SSC (at 65°C for 20 min), 0.2 × SSC (at 65°C for 30 min, twice), and PBST at room temperature (RT) for 10 min. Afterward, embryos were immunoreacted with an alkaline phosphatase (AP)-coupled anti-DIG antibody (1:8,000) and then stained with nitro blue tetrazolium (NBT) (Roche) and 5-bromo-4-chloro-3-indolyl phosphate (BCIP) (Roche) for the AP reaction in the AP system. Fluorescence staining was conducted with a commercial kit, TSA Plus Fluorescence Systems (Perkin-Elmer, Boston, MA, USA). Fluorescence signals detected by DIG-labeled RNA probes were amplified through fluorescein-tyramide signal amplification. Images were obtained with a microscope (Leica, Heidelberg, Germany).

Table 1. *Specific primer sequences of the quantitative real-time RT-PCR and in situ hybridization*

Gene Name	Forward Primer Sequence (5′-3′)	Reverse Primer Sequence (5′-3′)
qRT-PCR		
rpl7	GAGATCCGCCTGGCTCGTA	GGGCTGACTCCGTTGATACCT
foxi3	GAACATAGAGCAAGGGCAAACAT	CGTCGTGGGCGTCTTAACGT
slc9a2	ATCGTCTGTTGTGCCCTC	CAGTTCCACTCGTGCTCT
slc9a3	ATGCCTGATGTCACTGCT	GTGTCGGTGCTGCTTCCT
atp6v1a	ACAAGTGCGCCCAGTAAC	CCCGAAGGCTCCAGGTAT
rhcg1	TGGGAGATGATGGGAAGATAAGC	GCAATGCTCCATAGGCAATCAA
In situ hybridization		
slc9a2	CTGCCATCTTTCTCAGGTTTTCAT	GGAGATGGCAAAGAGCTCAGCTAC
slc9a3	GCGCTGTGGATCCTGGTCTGTTGG	GTAGGACAGGTATCCCACCACAAA
atp6v1a	TTTGTGCATGGAGTTTCAGGACCA	GATCACAGTTTTTCCACACCCGAA

qRT-PCR, quantitative RT-PCR.

Whole-mount immunocytochemistry. For triple-labeling with *slc9a3* mRNA, Na^+-K^+-ATPase (NKA), and H^+-ATPase, medaka samples were first in situ hybridized and subsequently subjected to immunohistochemical treatments. After being washed with PBS, the in situ-hybridized samples were incubated with 3% BSA for 2 h to block nonspecific binding. Samples were then incubated overnight at 4°C with an α5 monoclonal antibody against the avian NKA (Developmental Studies Hybridoma Bank, University of Iowa, Ames, IA), and a polyclonal antibody against the A subunit of killifish H^+-ATPase (27). After being washed with PBS for 20 min, samples were further incubated in Alexa Fluor 488 goat anti-rabbit immunoglobulin G (IgG; Molecular Probes, Invitrogen, Carlsbad, CA; diluted 1:200 with PBS) and Alexa Fluor 568 goat anti-mouse IgG antibodies (Molecular Probes; diluted 1:200 with PBS) for 2 h at room temperature. For double-labeling with NHE3 and NKA, embryos were fixed and immunolabeled with an affinity-purified anti-NHE3 polyclonal antibody and NKA antibody. The anti-NHE3 antibody was generated in rabbits injected with a 16-residue synthetic peptide (^{730}VAPSQRAQTRPPLTAG^{745}) of NHE3, used at a dilution of 1:100. Images were acquired with a Leica TCS-SP5 confocal laser scanning microscope (Leica Lasertechnik, Heidelberg, Germany). For z-plan images, 30 serial sections (0.5 μm/section; at a total thickness of 15 μm) of confocal microscopic images were acquired and subjected to image reconstruction and analysis.

Western blot analysis. Western blotting was carried out to characterize the anti-NHE3 antibody generated in our laboratory. Protein samples (50 mg/well) were loaded for 10% SDS-PAGE at 100 V for 2 h. After separation, proteins were transferred to polyvinylidene difluoride membranes (Millipore, Billerica, MA) at 100 V for 2 h. After being blocked for 1.5 h in 5% nonfat milk, blots were incubated with an anti-NHE3 antibody (overnight at 4°C, diluted 1:250) and with an AP-conjugated goat anti-rabbit IgG antibody (diluted 1:5,000, at room temperature; Jackson Laboratories, West Grove, PA) for another 2 h. Blots were developed with BCIP/NBT.

Scanning ion-selective electrode technique (SIET). H^+-, NH_4^+-, and Na^+-selective microelectrodes were constructed to measure ionic activities at the apical surface of individual MR cells and keratinocytes in the yolk-sac area of intact medaka embryos. Glass capillary tubes (no. TW 150–4; World Precision Instruments, Sarasota, FL) were pulled on a Sutter P-97 Flaming Brown pipette puller (Sutter Instruments, San Rafael, CA) into micropipettes with tip diameters of 3–5 μm. These were baked at 120°C overnight and vapor-sialanized with dimethyl chlorosilane (Sigma-Aldrich) for 30 min. Before use, the micropipettes were backfilled with a 1-cm column of electrolytes and frontloaded with a 20- to 30-μm column of a liquid ion exchanger cocktail (Sigma-Aldrich) to create an ion-selective microelectrode (probe). The following ionophore cocktails (and electrolytes) were used: H^+ ionophore I cocktail B (40 mM KH_2PO_4 and 15 mM K_2HPO_4; pH 7); Na^+ ionophore II cocktail A (100 mM NaCl); and NH_4^+ ionophore I cocktail B (100 mM NH_4Cl). The ion-selective microelectrode was connected to an operational amplifier (IP Amp ion polarographic amplifier; Applicable Electronics, East Falmouth, MA) via an Ag/AgCl wire electrode holder (World Precision Instruments), and the circuit was completed by placing a salt bridge (3 M potassium acetate, 10 mM KCl in 3% agarose connected to a Ag/AgCl wire). Electrode vibration and positioning were achieved with a stepper motor-driven three-dimensional (3D) positioner (Applicable Electronics). Data acquisition, preliminary processing, and control of the 3D electrode positioner were performed with ASET software (Science Wares, East Falmouth, MA). To calibrate the ion-selective probe, the Nernstian property of each microelectrode was measured by placing the microelectrode in a series of standard solutions (pH 6, 7, and 8 for the H^+ probe; 0.1, 1, and 10 mM NaCl for the Na^+ probe; and 0.1, 1, and 10 mM NH_4Cl for the NH_4^+ probe). By plotting the voltage output of the probe against log [H^+], [Na^+], and [NH_4^+] values, linear regressions gave Nernstian slopes of 58.3 ± 0.7 (n = 10) for H^+, 57.5 ± 0.5 (n = 10) for Na^+, and 58 ± 0.6 (n = 10) for NH_4^+. According to technical documents published on the Sigma website (www.sigmaaldrich.com), the selectivity coefficients of the Fluka NH_4^+ ionophore I cocktail B is only four times more selective to NH_4^+ than to K^+. To prevent interference from K^+ in the medium, K^+-free recording medium was used when probing NH_4^+. Because the calibration (Nernstian) slope of NH_4^+ gradually decayed at concentrations of <0.1 mM, the NH_4^+ concentration in the recording medium was raised by adding 0.05 mM $(NH_4)_2SO_4$ for a practical and precise calibration (36).

Measurements of H^+, Na^+, and NH_4^+ fluxes at specific cells. The SIET was performed at room temperature (26–28°C) in a small plastic recording chamber filled with 2 ml of FW recording medium. The FW recording medium contained artificial FW, 300 μM MOPS buffer, and 0.3 mg/l ethyl 3-aminobenzoate methanesulfonate (Tricaine, Sigma-Aldrich). The pH of the FW-recording medium was adjusted to 7.0 by adding an NaOH or HCl solution. Before measurement, an anesthetized larva was positioned in the center of the chamber with its lateral side contacting the base of the chamber. To record ionic gradients at the apical surface of the MR cells, the microelectrode was moved to a position about 2–3 μm above the apical surface of the cell. Voltage differences in microvolts were recorded by probing orthogonally to the surface at 10-μm intervals. The recording was performed on a cell for five replicates, and the median value was used to calculate the ionic fluxes of the cell using ASET software, as described in previous reports (11, 36, 37).

Statistical analysis. Values are presented as the means ± SD and were compared using Student's t-test. A significant difference of $P < 0.05$ was used between the treatment and control groups.

RESULTS

Localization of NHE, H^+-ATPase, and NKA. Whole-mount in situ hybridization was used to detect mRNA expressions of *slc9a2*, *slc9a3*, and *atp6v1a* in 7-dpf medaka embryos. *slc9a2* showed no signal on the yolk sac or pharyngeal arches of the medaka embryo; however, *slc9a3* revealed strong signals in specific cells on the skin of the yolk sac and pharyngeal arches (Fig. 1, *A* and *B*). On the other hand, *atp6v1a* mRNA was expressed in pharyngeal arches but had very weak signals on the yolk sac (Fig. 1*C*).

In previous studies, an NKA antibody was used to detect MR cells on the yolk sac and skin of 7-dpf medaka embryos (36, 45). In this study, we used the same NKA antibody to double-stain with *slc9a3* mRNA (fluorescent in situ hybridization), and results showed the colocalization of both signals in a group of MR cells (Fig. 2, *A–C*). Double immunostaining with the anti-NHE3 and anti-NKA antibodies showed apical NHE3 and basolateral NKA protein signals in the same MR cells (Fig. 2, *D–F*, *J*, *K*). On the other hand, H^+-ATPase was only expressed in a few MR cells with a basolateral pattern (Fig. 2, *G–I*, *L*, *M*). In Western blots for characterizing anti-NHE3 antiserum, results revealed an immunoreactive band of 110 kDa that was not observed after the antibody was incubated with excess synthetic peptide (to raise the antibody) or with preimmune serum incubation (Fig. 2*N*). The size of the band was larger than expected on the basis of the predicted medaka NHE3 (84 kDa) sequence.

To further distinguish NHE3$^-$ and H^+-ATPase-expressing MR cells, triple labeling of *slc9a3* mRNA, H^+-ATPase, and NKA was conducted in medaka gills. *slc9a3* mRNA and H^+-ATPase protein were both colocalized on NKA-labeled MR cells (Fig. 3, *A* and *B*). However, *slc9a3* mRNA and H^+-ATPase protein were expressed in different MR cells, indicating that there were at

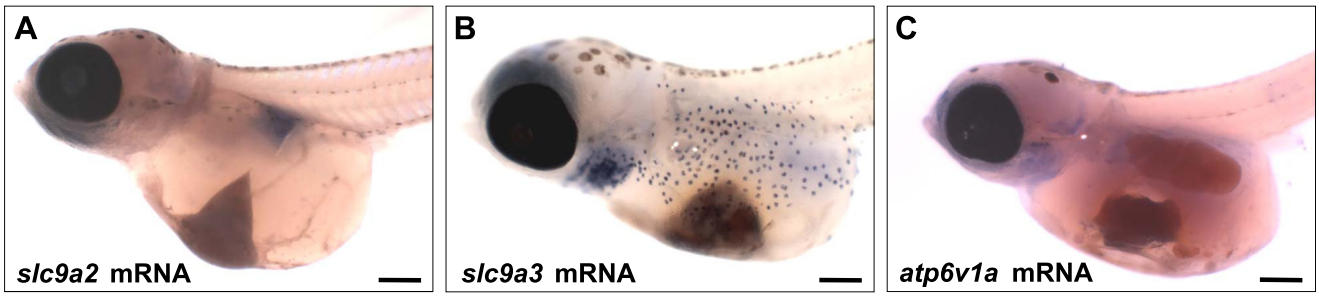

Fig. 1. Whole-mount in situ hybridization of *slc9a2* (*A*), *slc9a3* (*B*), and *atp6v1a* (*C*) mRNAs in 7-day postfertilization (dpf) medaka embryos. *A*: No *slc9a2* mRNA signal was detected on the yolk sac or pharyngeal arch. *B*: *slc9a3* mRNA signals were detected in a group of ionocytes on the yolk sac and pharyngeal arch. *C*: *atp6v1a* mRNA signals were localized on the pharyngeal arch and were very weak on the yolk sac. Scale bar: 200 μm.

least two distinct subtypes of MR cells: NHE3- and H^+-ATPase-expressing MR cells (Fig. 3, *C* and *D*).

Effects of acidic FW acclimation on slc9a2, slc9a3, atp6v1a, foxi3, and rhcg1 expressions. In pilot experiments, adult and embryo medaka were incubated in FW at various pH values, and their survival was examined. Adult medaka showed good acclimation in pH 4 but died in pH 3 water after 1 wk of treatment. Embryos showed weaker acid acclimation ability with good acclimation in pH 5 but death in pH 4 water. The body length of newly hatched embryos showed no significant

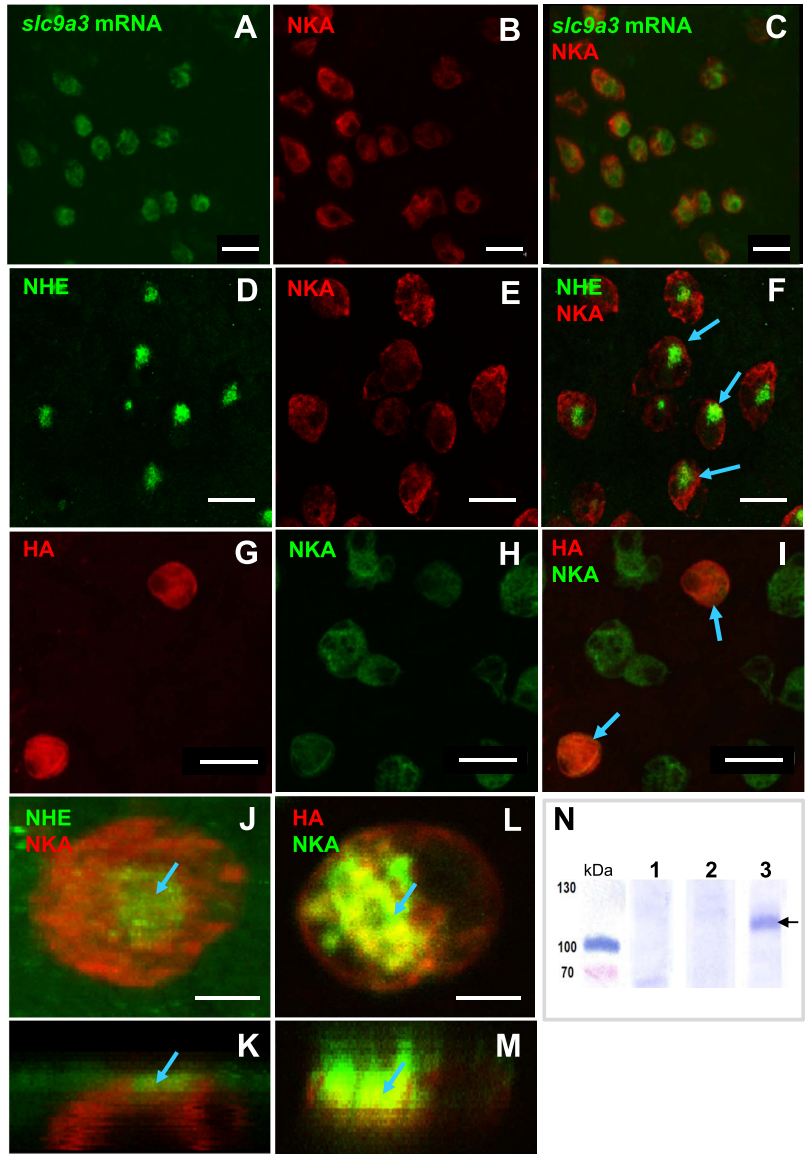

Fig. 2. Double-fluorescence in situ hybridization and immunocytochemistry of *slc9a3*, Na^+/H^+ exchanger 3 (NHE3), H^+-ATPase (HA), and Na^+-K^+-ATPase (NKA). *A*: *slc9a3* mRNA. *B*: NKA protein. *C*: merged image of *A* and *B*. *D*: NHE3 (NHE) protein. *E*: NKA protein. *F*: merged image of *D* and *E*. *G*: HA protein. *H*: NKA protein. *I*: merged image of *G* and *H*. Scale bar for *A*–*I*: 20 μm. *J*: colocalization of NHE and NKA proteins. *K*: Z-plane image of *J*. *L*: colocalization of HA and NKA proteins. *M*: Z-plane image of *L*. Scale bar for *J*–*M*: 5 μm. *N*: Western blot of NHE3. *slc9a3* mRNA was colocalized in NKA-labeled MR cells (*C*). NHE3 was expressed at the apical membrane of MR cells (arrows in *F*, *J*, and *K*). HA was expressed at the basolateral membrane of NKA-labeled MR cells (arrows in *I*, *L*, and *M*). Western blot of gill tissues with an anti-medaka NHE3 protein showed a 110-kDa immunoreactive band (*lane 3*). The band was absent when the antibody was preincubated with excess antigen peptide (*lane 2*) or replaced with preimmune serum (*lane 1*).

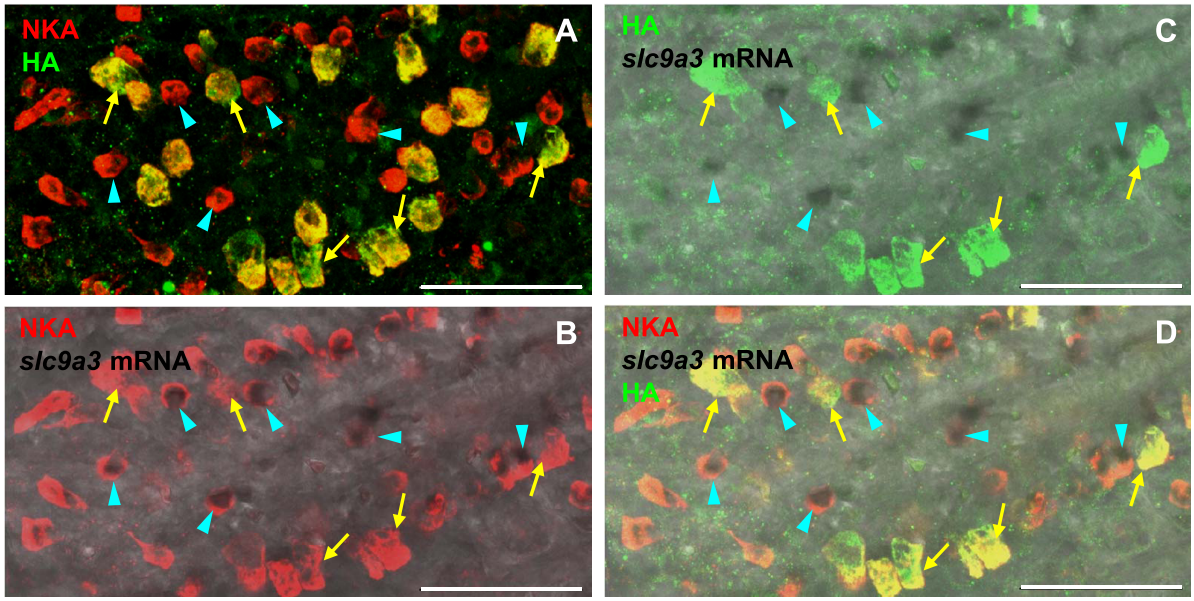

Fig. 3. Triple labeling of *slc9a3* mRNA with HA and NKA proteins in adult medaka gills. *Slc9a3* mRNA (black signal) (*A*) and HA protein (green signal) (*B*) were colocalized with the NKA signal (red signal). *slc9a3* mRNA (arrowheads) and HA protein (arrows) were expressed in different groups of NKA-labeled MR cells (*C*, *D*). Scale bar: 50 μm.

difference between pH 5 and pH 7 FW (data not shown). Therefore, the acid acclimation applied in the following experiment was pH 4 for adult fish for 2 wk and pH 5 for embryos from fertilization to hatching.

A qRT-PCR was used to examine the effect of acid acclimation on mRNA expressions of *slc9a2*, *slc9a3, atp6v1a, foxi3,* and *rhcg1* in adult gills. mRNA expression of *slc9a3* was upregulated by about three-fold in gills after acid acclimation (Fig. 4*A*). *atp6v1a* mRNA expression also increased after acid acclimation; however, the quantity was much lower than that of *slc9a3* (Fig. 4*C*). The expression of *slc9a2* mRNA was low and exhibited no significant difference between the normal FW control and treatment groups (Fig. 4*B*). Similar to *slc9a3* and *atp6v1a,* transcription of *foxi3* and *rhcg1* was also stimulated by acid acclimation (Fig. 4, *D* and *E*).

In embryos, the signal and cell density of *slc9a3* mRNA-expressing MR cells on the yolk sac both significantly increased after acid acclimation (Fig. 5). Supporting the data of Fig. 5, the density of NHE3-expressing MR cells also increased after acid acclimation (Fig. 6). Notably, the number of H^+-ATPase-expressing MR cells also increased after acid acclimation (Fig. 7). However, the density of H^+-ATPase-expressing MR cells was much lower than that of NHE3-expressing MR cells (Figs. 6 and 7).

Ionic fluxes at MR cells and keratinocytes of yolk-sac skin of embryos. The SIET was used to measure net Na^+, H^+, and NH_4^+ fluxes (measured at 2 orthogonal positions at 10-μm intervals) at the surface of individual MR cells and adjacent keratinocytes in embryos acclimated to normal or acidic FW (pH 5). Results showed that the outward NH_4^+ flux (NH_4^+ excretion) and inward Na^+ flux (Na^+ uptake) of MR cells were both induced after acid acclimation (Fig. 8, *B* and *C*); however, the H^+ flux did not significantly change (Fig. 8*A*). In keratinocytes, ionic fluxes were significantly lower than those in MR cells, and only the outward Na^+ flux was stimulated by acid acclimation (Fig. 8*C*). In this experiment, most MR cells measured were acid-secreting cells; therefore, data of base-secreting cells are not shown (48).

DISCUSSION

In the present study, we first found that there were apical NHE3-expressing MR cells and basolateral H^+-ATPase-expressing MR cells in the FW-acclimated euryhaline teleost,

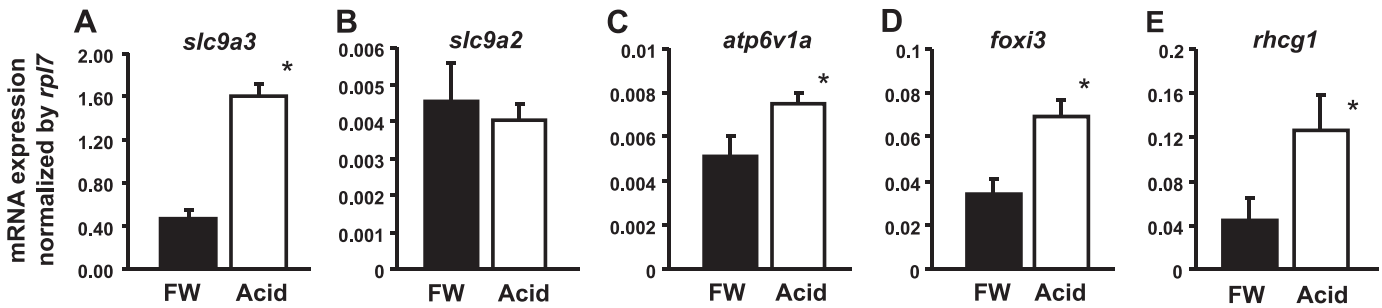

Fig. 4. qRT-PCR analysis of the effects of normal and acidic freshwater (FW) acclimation on *slc9a3* (*A*), *slc9a2* (*B*), *atp6v1a* (*C*), *foxi3* (*D*), and *rhcg1* (*E*) mRNA expressions in gills of adult fish. *slc9a3, foxi3*, *atp6v1a,* and *rhcg1* mRNA expressions increased after acid acclimation, but that of *slc9a2* did not change. Values were normalized by *rpl7*. Values are expressed as means ± SD ($n = 6$). *Significant difference (Student's *t*-test, $P < 0.05$).

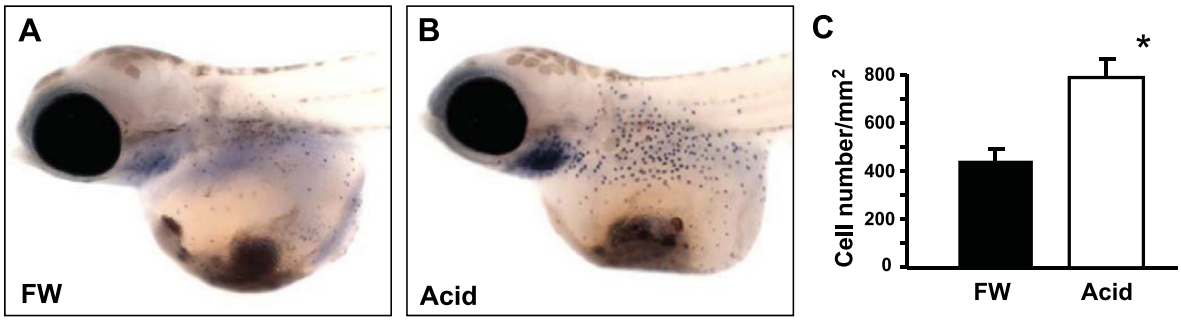

Fig. 5. Whole-mount *in-situ* hybridization of *slc9a3* on 7-dpf medaka embryos acclimated to normal (*A*) and acidic (*B*) FW. (*C*) Cell densities of *slc9a3*-expressing cells on the yolk sac. The cell density of *slc9a3*-expressing cells increased after acclimation. Mean ± SD (n = 20). *Significant difference (Student's t-test, $P < 0.05$).

medaka. Increases in NHE3-expressing MR cells, NHE3/Rhcg1 mRNA, and Na^+ uptake/NH_4^+ excretion after acid acclimation suggested that the NHE3/Rhcg1-mediated Na^+ uptake/NH_4^+ excretion mechanism plays a critical role in acidic equivalent (H^+/NH_4^+) excretion by FW medaka.

The molecular identity and cellular localization of NHE isoforms and H^+-ATPase were well reported in the marine dogfish (*Squalus acanthias*) and longhorn sculpin (*Myoxocephalus octodecemspinosus*) and euryhaline stingray (*Dasyatis sabina*), and two distinct ionocytes, one expressing apical NHE3/2 and the other basolateral HA, were consistently identified and proposed as conducting acid and base secretion, respectively (6, 8, 9, 10, 33, 40, 41). Similar to those species, medaka, a euryhaline teleost, also has two distinct ionocytes, apical NHE3- and basolateral H^+-ATPase-expressing MR cells, in FW environments. On the other hand, both NHE3b and H^+-ATPase were apically localized to the same type of ionocyte, HR cells, in the stenohaline FW zebrafish (21, 22, 23, 49). In FW-acclimated tilapia and Osorezan dace, the NHE was found to be expressed in apical membranes of a group of MR cells, while localization of H^+-ATPase has not been elucidated (14, 16, 24). In FW-acclimated rainbow trout, NHE2 mRNA and the apical NHE3 protein were localized in gill PNA^+ MR cells (25), while apical H^+-ATPase was found in pavement cells (probably PNA^- MR cells) (15, 38). In the case of FW-acclimated killifish, H^+-ATPase was reported to be expressed in basolateral membranes of MR cells (27), but the cellular localization of NHE isoforms has not been clarified. Taken together, cellular localization of NHEs and H^+-ATPase in ionocytes is considerably diverse among FW teleosts. Euryhaline teleosts (like medaka and rainbow trout) develop two distinct types of ionocytes (NHE- and H^+-ATPase-expressing MR cells), as do euryhaline elasmobranchs and marine teleosts. On the other hand, stenohaline FW teleosts, like zebrafish, coexpress both NHE3 and H^+-ATPase in the same ionocytes; however, more species need to be studied by double-localization approaches to support this notion.

Several experiments provided evidence for the physiological role of NHE3 in medaka. First, acclimation to acidic FW induced NHE3 mRNA expression in medaka gills (Fig. 4*A*), and the number of the NHE3 MR cells in embryonic skin increased (Fig. 5). Outward H^+ gradients at MR cells (mostly NHE3-expressing cells) were much higher, by about 23-fold, than those of keratinocytes. Moreover, our previous study (48) indicated inhibitory effects of 100–1,000 μM EIPA (an NHE inhibitor) on H^+ fluxes at MR cells in medaka embryonic skin. Notably, NHE3-expressing MR cells appeared to dominate (about 95%, estimated from Figs. 6*E* and 7*E*) over the others (e.g., basolateral H^+-ATPase-expressing MR cells) in cell

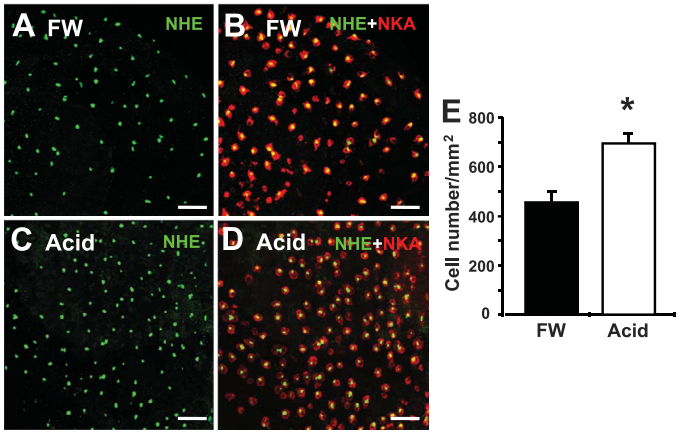

Fig. 6. Double-fluorescence immunocytochemistry of NHE3 (NHE, green signal; *A*, *C*) and the NKA protein (red signal; *B*, *D*) in 7-dpf embryos acclimated to normal (*A*, *B*) and acidic FW (*C*, *D*). *E*: cell densities of NHE3-expressing cells on the yolk sac. The NHE3-expressing MR cell number increased after acid acclimation. Scale bar: 50 μm. Values are expressed as means ± SD (n = 6). *Significant difference (Student's t-test, $P < 0.05$).

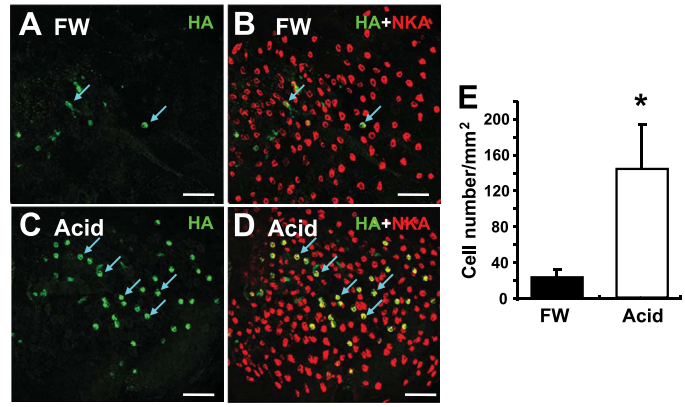

Fig. 7. Double-fluorescence immunocytochemistry of HA (green signal; *A* and *C*) and the NKA protein (red signal; *B* and *D*) in 7-day dpf embryos acclimated to normal FW (*A* and *B*) and acidic FW (acid) (*C* and *D*). *E:* cell densities of HA-expressing cells on the yolk sac. The HA-expressing MR cell number increased after acid acclimation. Scale bar: 50 μm. Values are expressed as means ± SD (n = 5). *Significant difference (Student's t-test, $P < 0.05$).

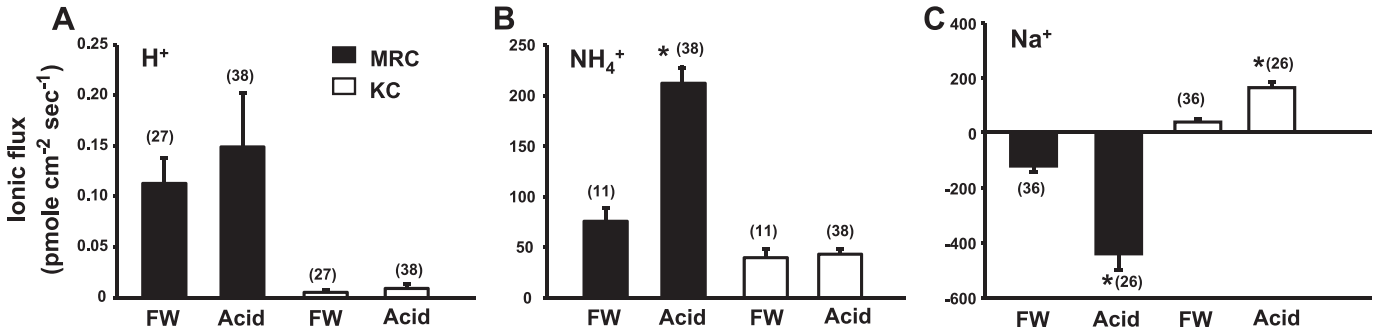

Fig. 8. H^+ fluxes (*A*), NH_4^+ fluxes (*B*), and Na^+ fluxes (*C*) at MR cells (MRC) and keratinocytes (KC) on the skin of medaka embryos acclimated to normal or acidic FW. Data are presented as the means ± SD (*n* shown in parentheses). *Significant difference between the normal FW and acid groups (Student's *t*-test, $P < 0.05$).

number among NKA-labeled MR cells. More importantly, 100 μM bafilomycin (an H^+-ATPase inhibitor) could not suppress H^+ fluxes at MR cells (48). Taken together, apical NHE3, but not basolateral H^+-ATPase, is one of the major players carrying out acid secretion function in medaka skin and gills. On the other hand, H^+-ATPase was only reported to be expressed in basolateral membranes of MR cells in the euryhaline stingray, marine fishes (6, 9, 35, 46), and one euryhaline teleost, the killifish (27). These basolateral H^+-ATPase-expressing MR cells were suggested to be involved in base secretion and/or Cl^- uptake. In the present study, the cell number of H^+-ATPase-expressing MR cells and H^+-ATPase mRNA both increased after acid acclimation; however, their quantities were still much lower than those of NHE3-expressing MR cells (Figs. 4 and 7). As suggested above, H^+-ATPase-expressing MR cells might not play a major role in medaka acid excretion, and more proteins like the Cl^-/HCO_3^- exchangers and carbonic anhydrase have to be examined in the future to clarify the functions of H^+-ATPase-expressing MR cells.

As described above, the functional roles of NHEs in the acid-secretion mechanism in FW teleosts have been investigated for a long time; however, most previous studies provided only fragmentary evidence. In tilapia and Osorezan dace, acclimation to acidic FW-stimulated NHE3 mRNA expression and the number and size (only in tilapia) of NHE3-expressing MR cells (14, 16); however, data of the acid secretion function of MR cells are not available to support their molecular and cellular evidence. In rainbow trout, both the NHE3 protein and NHE2 mRNA were expressed by gill PNA^+ cells, but only NHE2 mRNA was upregulated in gills after hypercapnic treatment (25). Accordingly, NHE2 was proposed to be the major member of SLC9A, contributing to the acid-base regulatory mechanism in rainbow trout gills (25). In most FW teleosts studied (medaka, Osorezan dace, tilapia, and zebrafish), NHE3 (or NHE3b) is the major isoform involved in gill ionoregulatory mechanisms, as in mammals in which NHE3 is the major player carrying out about 70–80% of Na^+/HCO_3^- reabsorption in nephrons (45). In the case of rainbow trout, there are 2 subtypes of SLC9A3, rtNHE3a (NM_001130995.1) (25), and -b (NM_001160482.1), found in genetic databases (NCBI), and rtNHE3b shows a higher homology (59.8%) with zebrafish NHE3b than does rtNHE3a (53%). An anti-rtNHE3 antibody, which likely recognizes both NHE3a and -b, was used to localize the protein signals in trout gill MR cells (25). Only NHE3a-specific primers were used for the real-time PCR analysis, which indicated no changes in gill NHE3 transcripts after hypercapnic treatment (25). However, the possibility of the involvement of rtNHE3b in trout acid-base regulatory mechanisms in FW cannot be excluded without further cellular localization and functional analyses with convincing molecular physiological approaches.

Considering thermodynamic constraints, the function of the electroneutral apical NHE in most FW environments has long been questioned (23, 31). The identification of an ammonia transporter, Rhcg1, in zebrafish and a functional assay of zebrafish, HR cells provided evidence to support the hypothesis that the proton gradient created by apical H^+-ATPase and/or NHE3b drives facilitative NH_3 diffusion through the Rhcg1 (22, 30, 36). Wood and Wright and colleagues (42, 47) used cultured rainbow trout gill and kinetics experiments to propose a model of an apical "Na^+/NH_4^+ exchange complex" (metabolon model), in which H^+-ATPase, NHE, Na^+-channel, and Rh glycoprotein are involved. However, these proteins were not demonstrated in the same MR cells. Wu et al. (48) and Shih et al. (36) further provided clear molecular and functional evidence to show that the coupling of NHE3 and Rhcg1 in MR cells plays a critical role in NH_4^+-dependent Na^+ uptake. They found that both NHE3 and Rhcg1 were located in MR cells, and their mRNA levels were upregulated by low-Na^+ water acclimation (48). Following that study, Kumai and Perry (28) also suggested a functional coupling of NHE3 and Rhcg1 for Na^+ uptake in zebrafish acclimated to acidic water (pH 4). However, they did not report whether NHE3 and Rhcg1 are upregulated by acid acclimation. In the present study, acid acclimation upregulated mRNA expression of NHE3 and Rhcg1 in adult gills. It also increased NH_4^+ excretion and Na^+ uptake by embryonic skin MR cells, suggesting that NHE3/Rhcg1 coupling in apical membranes of MR cells plays a critical role in excreting acidic equivalents (H^+/NH_4^+). For the first time, Rhcg1 was found to be upregulated by acid acclimation. In apical membranes of MR cells, operation of the electroneutral NHE3 may be driven down the H^+ gradient that is created by deprotonation of NH_4^+ through Rhcg1 (22, 23, 48). During acid acclimation, enhanced nonionic NH_3 excretion through Rhcg1 would consume more H^+ and thus drive more Na^+/H^+ exchange through NHE3, consequently excreting excess acidic equivalents (H^+/NH_4^+). This could explain why the H^+ gradient at MR cells did not change after acid acclimation (Fig. 8*A*). However, other acid-base buffering

systems, like the HCO_3^- reabsorption mechanism, may also consume part of the H^+.

Similar to zebrafish (18), medaka enhance their acid secretion function by not only increasing the number of acid-secreting ionocytes (Fig. 6) but also stimulating the functional capacity at each ionocyte (Fig. 8). In medaka, the functional regulation at each NHE3 ionocyte may be achieved by regulating activity and/or mRNA expression of the relavant transporters if we compare the data of ionocyte number and transporter mRNA expressions. The number of NHE3-expressing cells was increased 1.3-fold (estimated from Fig. 6) after acid acclimation, while mRNA expressions of NHE3 and Rhcg1 were stimulated about 2.9–3.4 times (estimated from Fig. 4), suggesting an upregulation of the transporter mRNA expressed at each ionocyte.

One remarkable function of mammalian kidneys is to excrete net acid in the urine when experiencing a sustained increment in acid loading (4). Recent studies also found that apical H^+-ATPase and Rhcg play critical roles in excreting acid equivalents (H^+/NH_4^+) by collecting duct-intercalated cells (43). Deletion of an Rhcg strongly reduced renal ammonium secretion, caused metabolic acidosis in acid-challenged mice, and impaired restoration of a normal acid-base status (2, 43).

In mammals, chronic acid loads (hours to days) induce the appearance of cells positive for the proliferation markers BrdU, PCNA, or Ki67 in the collecting duct, suggesting the proliferation of acid-secreting, α-intercalated cells (44). Chronic acid adaptation can increase the NHE3 protein and activity in proximal tubules through the Pyk2/c-Src pathway (4). However, no study has shown the effect of acid loading on the cell number of proximal tubules. In the collecting duct, the transcription factor, *foxi1,* was identified to have a critical role in determining cell differentiation (1). Foxi1$^{-/-}$ mice lose the proper gene expression pattern needed to maintain an adequate acid-base homeostasis and thus develop distal renal tubular acidosis (3). In our previous study, the HR cell number increased after 4 days of acid acclimation through epithelial stem cell proliferation and ionocyte differentiation (19). An acidic environment simultaneously stimulated *zgcm2* mRNA expression, a specific transcription factor for HR cell differentiation in zebrafish, illustrating that this cell fate-related transcription factor may be involved in the chronic acid adaptation mechanism (7, 13, 20). *foxi3a* and *foxi3b* were demonstrated to act as main regulators for specification and differentiation of ionocytes in zebrafish skin/gills; knockdown of *zfoxi3a/3b* was found to block differentiation of all ionocytes (12, 20, 26). In medaka, *foxi3* is expressed in progenitor and differentiated MR cells (39). mRNA expression of *foxi3* also increased after acid acclimation (Fig. 4*D*), suggesting the involvement of *foxi3* in promoting differentiation of NHE3-expressing MR cells (and thus their function) to cope with an acidic environment.

Perspectives and Significance

Teleosts appear to have evolved two distinct pathways mediated by the apical NHE and apical H^+-ATPase, respectively, to carry out acid-secretion functions in FW. Medaka, dace, and tilapia are all euryhaline species and develop apical NHE3 in MR cells to excrete H^+, as do euryhaline elasmobranchs and marine teleosts. Stenohaline FW teleosts, like zebrafish, coexpress both NHE3 and H^+-ATPase in the same ionocytes but mainly employ apical H^+-ATPase for the acid-secretion function. In contrast to these general patterns, rainbow trout express apical NHE2 in PNA^+ MR cells and apical H^+-ATPase in PNA^- MR cells, and both transporters were proposed to be involved in the acid-secretion mechanism. Further studies with convincing molecular physiological approaches, and on more species, are needed to explore the evolutional physiological significance of the two distinct acid-secretion mechanisms in FW teleosts.

ACKNOWLEDGMENTS

This study was financially supported by the grants to P. P. Hwang from Academia Sinica and the National Science Council, Taiwan, Republic of China. We thank Y. C. Tung for her assistance during the experiments.

DISCLOSURES

No conflicts of interest, financial or otherwise, are declared by the authors.

AUTHOR CONTRIBUTIONS

Author contributions: C.-C.L., L.-Y.L., H.-H.H., and J.-L.H. performed experiments; C.-C.L., L.-Y.L., H.-H.H., and J.-L.H. analyzed data; C.-C.L., L.-Y.L., V.T., P.P., J.-L.H., and P.-P.H. interpreted results of experiments; C.-C.L., H.-H.H., J.-L.H., and P.-P.H. prepared figures; C.-C.L. and J.-L.H. drafted manuscript; L.-Y.L., J.-L.H., and P.-P.H. edited and revised manuscript; V.T., P.P., J.-L.H., and P.-P.H. conception and design of research; P.-P.H. approved final version of manuscript.

REFERENCES

1. **Al-Awqati Q, Schwartz GJ.** A fork in the road of cell differentiation in the kidney tubule. *J Clin Invest* 113: 1528–1530, 2004.
2. **Biver S, Belge H, Bourgeois S, Van Vooren P, Nowik M, Scohy S, Houillier P, Szpirer J, Szpirer C, Wagner CA, Devuyst O, Marini AM.** A role for Rhesus factor Rhcg in renal ammonium excretion and male fertility. *Nature* 456: 339–343, 2008.
3. **Blomqvist SR, Vidarsson H, Fitzgerald S, Johansson BR, Ollerstam A, Brown R, Persson AE, Bergström GG, Enerbäck S.** Distal renal tubular acidosis in mice that lack the forkhead transcription factor Foxi1. *J Clin Invest* 113: 1560–1570, 2004.
4. **Bobulescu IA, Moe OW.** Na^+/H^+ exchangers in renal regulation of acid-base balance. *Semin Nephrol* 26: 334–344, 2006.
5. **Bobulescu IA, Moe OW.** Luminal Na^+/H^+ exchange in the proximal tubule. *Pflügers Arch* 458: 5–21, 2009.
6. **Catches JS, Burns JM, Edwards SL, Claiborne JB.** Na^+/H^+ antiporter, V-H^+-ATPase and Na^+/K^+-ATPase immunolocalization in a marine teleost (*Myoxocephalus octodecemspinosus*). *J Exp Biol* 209: 3440–3447, 2006.
7. **Chang WJ, Horng JL, Yan JJ, Hsiao CD, Hwang PP.** The transcription factor, glial cell missing 2, is involved in differentiation and functional regulation of H^+-ATPase-rich cells in zebrafish (*Danio rerio*). *Am J Physiol Regul Integr Comp Physiol* 296: R1192–R1201, 2009.
8. **Choe KP, Edwards SL, Claiborne JB, Evans DH.** The putative mechanism of Na^+ absorption in euryhaline elasmobranchs exists in the gills of a stenohaline marine elasmobranch, *Squalus acanthias*. *Comp Biochem Physiol A Mol Integr Physiol* 146: 155–162, 2007.
9. **Choe KP, Kato A, Hirose S, Plata C, Sindic A, Romero MF, Claiborne JB, Evans DH.** NHE3 in an ancestral vertebrate: primary sequence, distribution, localization, and function in gills. *Am J Physiol Regul Integr Comp Physiol* 289: R1520–R1534, 2005.
10. **Claiborne JB, Choe KP, Morrison-Shetlar AI, Weakley JC, Havird J, Freiji A, Evans DH, Edwards SL.** Molecular detection and immunological localization of gill Na^+/H^+ exchanger in the dogfish (*Squalus acanthias*). *Am J Physiol Regul Integr Comp Physiol* 294: R1092–R1102, 2008.
11. **Donini A, O'Donnell MJ.** Analysis of Na^+, Cl^-, K^+, H^+ and NH_4^+ concentration gradients adjacent to the surface of anal papillae of the mosquito *Aedes aegypti*: application of self-referencing ion-selective microelectrodes. *J Exp Biol* 208: 603–610, 2005.
12. **Esaki M, Hoshijima K, Kobayashi S, Fukuda H, Kawakami K, Hirose S.** Visualization in zebrafish larvae of Na^+ uptake in mitochondria-rich

cells whose differentiation is dependent on *foxi3a*. *Am J Physiol Regul Integr Comp Physiol* 292: R470–R480, 2007.
13. **Esaki M, Hoshijima K, Nakamura N, Munakata K, Tanaka M, Ookata K, Asakawa K, Kawakami K, Wang W, Weinberg ES, Hirose S.** Mechanism of development of ionocytes rich in vacuolar-type H^+-ATPase in the skin of zebrafish larvae. *Dev Biol* 329: 116–129, 2009.
14. **Furukawa F, Watanabe S, Inokuchi M, Kaneko T.** Responses of gill mitochondria-rich cells in Mozambique tilapia exposed to acidic environments (pH 4.0) in combination with different salinities. *Comp Biochem Physiol A Mol Integr Physiol* 158: 468–476, 2011.
15. **Galvez F, Reid SD, Hawkings G, Goss GG.** Isolation and characterization of mitochondria-rich cell types from the gill of freshwater rainbow trout. *Am J Physiol Regul Integr Comp Physiol* 282: R658–R668, 2002.
16. **Hirata T, Kaneko T, Ono T, Nakazato T, Furukawa N, Hasegawa S, Wakabayashi S, Shigekawa M, Chang MH, Romero MF, Hirose S.** Mechanism of acid adaptation of a fish living in a pH 3.5 lake. *Am J Physiol Regul Integr Comp Physiol* 284: R1199–R1212, 2003.
18. **Horng JL, Lin LY, Huang CJ, Katoh F, Kaneko T, Hwang PP.** Knockdown of V-ATPase subunit A (*atp6v1a*) impairs acid secretion and ion balance in zebrafish (*Danio rerio*). *Am J Physiol Regul Integr Comp Physiol* 292: R2068–R2076, 2007.
19. **Horng JL, Lin LY, Hwang PP.** Functional regulation of H^+-ATPase-rich cells in zebrafish embryos acclimated to an acidic environment. *Am J Physiol Cell Physiol* 296: C682–C692, 2009.
20. **Hsiao CD, You MS, Guh YJ, Ma M, Jiang YJ, Hwang PP.** A positive regulatory loop between *foxi3a* and *foxi3b* is essential for specification and differentiation of zebrafish epidermal ionocytes. *PLoS One* 2: e302, 2007.
21. **Hwang PP, Lee TH.** New insights into fish ion regulation and mitochondrion-rich cells. *Comp Biochem Physiol A Mol Integr Physiol* 148: 479–497, 2007.
22. **Hwang PP, Lee TH, Lin LY.** Ion regulation in fish gills: recent progress in the cellular and molecular mechanisms. *Am J Physiol Regul Integr Comp Physiol* 301: R28–R47, 2011.
23. **Hwang PP, Perry S.** Ionic and acid-base regulation. In: *Zebrafish, Fish Physiology Series*, edited by Perry S, Ekker, M, Farrell, AP, Brauner, CJ. San Diego, CA: Academic, p. 311–314, 2010.
24. **Inokuchi M, Hiroi J, Watanabe S, Hwang PP, Kaneko T.** Morphological and functional classification of ion-absorbing mitochondria-rich cells in the gills of Mozambique tilapia. *J Exp Biol* 212: 1003–1010, 2009.
25. **Ivanis G, Esbaugh AJ, Perry SF.** Branchial expression and localization of SLC9A2 and SLC9A3 sodium/hydrogen exchangers and their possible role in acid-base regulation in freshwater rainbow trout (*Oncorhynchus mykiss*). *J Exp Biol* 211: 2467–2477, 2008.
26. **Jänicke M, Carney TJ, Hammerschmidt M.** Foxi3 transcription factors and Notch signaling control the formation of skin ionocytes from epidermal precursors of the zebrafish embryo. *Dev Biol* 307: 258–271, 2007.
27. **Katoh F, Hyodo S, Kaneko T.** Vacuolar-type proton pump in the basolateral plasma membrane energizes ion uptake in branchial mitochondria-rich cells of killifish *Fundulus heteroclitus*, adapted to a low ion environment. *J Exp Biol* 206: 793–803, 2003.
28. **Kumai Y, Perry SF.** Ammonia excretion via Rhcg1 facilitates Na^+ uptake in larval zebrafish, *Danio rerio*, in acidic water. *Am J Physiol Regul Integr Comp Physiol* 301: 1517–1528, 2011.
29. **Lin LY, Horng JL, Kunkel JG, Hwang PP.** Proton pump-rich cell secretes acid in skin of zebrafish larvae. *Am J Physiol Cell Physiol* 290: C371–C378, 2006.
30. **Nakada T, Hoshijima K, Esaki M, Nagayoshi S, Kawakami K, Hirose S.** Localization of ammonia transporter Rhcg1 in mitochondrion-rich cells of yolk sac, gill, and kidney of zebrafish and its ionic strength-dependent expression. *Am J Physiol Regul Integr Comp Physiol* 293: R1743–R1753, 2007.
31. **Parks SK, Tresguerres M, Goss GG.** Theoretical considerations underlying Na^+ uptake mechanisms in freshwater fishes. *Comp Biochem Physiol C Toxicol Pharmacol* 148: 411–418, 2008.
32. **Pholpramool C, Borwornpinyo S, Dinudom A.** Role of Na^+/H^+ exchanger 3 in the acidification of the male reproductive tract and male fertility. *Clin Exp Pharmacol Physiol* 38: 353–359, 2011.
33. **Piermarini PM, Evans DH.** Immunochemical analysis of the vacuolar proton-ATPase B-subunit in the gills of a euryhaline stingray (*Dasyatis sabina*): effects of salinity and relation to Na^+/K^+-ATPase. *J Exp Biol* 204: 3251–3259, 2001.
34. **Reid SD, Hawkings GS, Galvez F, Goss GG.** Localization and characterization of phenamil-sensitive Na^+ influx in isolated rainbow trout gill epithelial cells. *J Exp Biol* 206: 551–559, 2003.
35. **Reis-Santos P, McCormick SD, Wilson JM.** Ionoregulatory changes during metamorphosis and salinity exposure of juvenile sea lamprey (*Petromyzon marinus L.*). *J Exp Biol* 211: 978–988, 2008.
36. **Shih TH, Horng JL, Hwang PP, Lin LY.** Ammonia secretion in skin of zebrafish larvae *(Danio rerio*). *Am J Physiol Cell Physiol* 295: C1625–C1632, 2008.
36a. **Shih TH, Horng JL, Liu ST, Hwang PP, Lin LY.** Rhcg1 and NHE3b are involved in ammonium-dependent sodium uptake by zebrafish larvae acclimated to low-sodium water. *Am J Physiol Regul Integr Comp Physiol* 302: 84–93, 2012.
37. **Smith PJ, Hammar K, Porterfield DM, Sanger RH, Trimarchi JR.** Self-referencing, non-invasive, ion selective electrode for single cell detection of trans-plasma membrane calcium flux. *Microsc Res Tech* 46: 398–417, 1999.
38. **Sullivan GV, Fryer JN, Perry SF.** Immunolocalization of proton pumps (H^+-ATPase) in pavement cells of rainbow trout gill. *J Exp Biol* 198: 2619–2629, 1995.
39. **Thermes V, Lin CC, Hwang PP.** Expression of Ol-foxi3 and Na^+/K^+-ATPase in ionocytes during the development of euryhaline medaka (*Oryzias latipes*) embryos. *Gene Expr Patterns* 10: 185–192, 2010.
40. **Tresguerres M, Katoh F, Fenton H, Jasinska E, Goss GG.** Regulation of branchial V-H^+-ATPase, Na^+/K^+-ATPase and NHE2 in response to acid and base infusions in the Pacific spiny dogfish (*Squalus acanthias*). *J Exp Biol* 208: 345–354, 2005.
41. **Tresguerres M, Parks SK, Katoh F, Goss GG.** Microtubule-dependent relocation of branchial V-H^+-ATPase to the basolateral membrane in the Pacific spiny dogfish (*Squalus acanthias*): a role in base secretion. *J Exp Biol* 209: 599–609, 2006.
42. **Tsui TKN, Hung CYC, Nawata CM, Wilson JM, Wright PA, Wood CM.** Ammonia transport in cultured gill epithelium of freshwater rainbow trout: The importance of Rhesus glycoproteins and the presence of an apical Na^+/NH_4^+ exchange complex. *J Exp Biol* 212: 878–892, 2009.
43. **Wagner CA, Devuyst O, Belge H, Bourgeois S, Houillier P.** The rhesus protein RhCG: a new perspective in ammonium transport and distal urinary acidification. *Kidney Int* 79: 154–161, 2011.
44. **Wagner CA, Devuyst O, Bourgeois S, Mohebbi N.** Regulated acid-base transport in the collecting duct. *Pflügers Arch* 458: 137–156, 2009.
45. **Wagner CA, Finberg KE, Breton S, Marshansky V, Brown D, Geibel JP.** Renal vacuolar-ATPase. *Physiol Rev* 84: 1263–1314, 2004.
46. **Wilson JM, Laurent P, Tufts BL, Benos DJ, Donowitz M, Vogl AW, Randall DJ.** NaCl uptake by the branchial epithelium in freshwater teleost fish: an immunological approach to ion-transport protein localization. *J Exp Biol* 203: 2279–2296, 2000.
47. **Wright PA, Wood CM.** A new paradigm for ammonia excretion in aquatic animals: role of Rhesus (Rh) glycoproteins. *J Exp Biol* 212: 2303–2312, 2009.
48. **Wu SC, Horng JL, Hwang PP, Wen ZH, Lin CS, Lin LY.** Ammonium-dependent sodium uptake in mitochondrion-rich cells of medaka (*Oryzias latipes*) larvae. *Am J Physiol Cell Physiol* 298: C237–C250, 2010.
49. **Yan JJ, Chou MY, Kaneko T, Hwang PP.** Gene expression of Na^+/H^+ exchanger in zebrafish H^+-ATPase-rich cells during acclimation to low-Na^+ and acidic environments. *Am J Physiol Cell Physiol* 293: C1814–C1823, 2007.